

Micromachined bulk PZT tissue contrast sensor for fine needle aspiration biopsy

Tao Li,^{*a} Roma Y. Gianchandani^b and Yogesh B. Gianchandani^a

Received 4th August 2006, Accepted 6th November 2006

First published as an Advance Article on the web 23rd November 2006

DOI: 10.1039/b611233a

This paper describes a micromachined piezoelectric sensor, integrated into a cavity at the tip of a biopsy needle, and preliminary experiments to determine if such a device can be used for real-time tissue differentiation, which is needed for needle positioning guidance during fine needle aspiration (FNA) biopsy. The sensor is fabricated from bulk lead zirconate titanate (PZT), using a customized process in which micro electro-discharge machining is used to form a steel tool that is subsequently used for batch-mode ultrasonic micromachining of bulk PZT ceramic. The resulting sensor is 50 μm thick and 200 μm in diameter. It is placed in the biopsy needle cavity, against a steel diaphragm which is 300 μm diameter and has an average thickness of 23 μm . Devices were tested in materials that mimic the ultrasound characteristics of human tissue, used in the training of physicians, and with porcine fat and muscle tissue. In both schemes, the magnitude and frequency of an electrical impedance resonance peak showed tissue-specific characteristics as the needle was inserted. For example, in the porcine tissue, the impedance peak frequency changed ≈ 13 MHz from the initial 163 MHz, and the magnitude changed $\approx 1600 \Omega$ from the initial 2100 Ω , as the needle moved from fat to muscle. Samples including oils and saline solution were tested for calibration, and an empirical tissue contrast model shows an approximately proportional relationship between measured frequency shift and sample acoustic impedance. These results suggest that the device can complement existing methods for guidance during biopsies.

I. Introduction

Fine needle aspiration (FNA) biopsy is an extensively-used clinical procedure for the neck mass (thyroid, salivary gland, *etc.*), breast, lung, bone, kidney, and liver.¹ It is a minimally-invasive, cost-effective, and minor surgical procedure compared with other open surgical biopsy techniques,² and is used to extract tissue from the target region for subsequent cytological examination.

The FNA biopsy procedure can be challenging for the healthcare professional that is performing it, because of the precision required in acquiring the desired sample from the small target volumes. The needle used is usually 20–27 gauge, with an outer diameter of <1 mm. This is in order to obtain precise samples from the correct place, to minimize damage in the path of the needle, and to avoid collateral damage to surrounding features, such as the carotid artery in the case of a thyroid biopsy (Fig. 1). To guide the positioning of the needle in a thyroid biopsy, conventional ultrasound imaging is performed in real time, especially for those targets that are difficult to palpate or contain complicated solid and cystic areas. This adds significant complexity, requiring special training and equipment that is

not widely available, yet is not always effective in providing the necessary precision. For example, at least 2–5% of thyroid FNA biopsies are read as non-diagnostic because of improper sampling.^{3–5} A biopsy needle with integrated sensors that can detect different tissue planes or variations of densities (*e.g.*, solid *vs.* cystic) can provide effective guidance to the physician, making this procedure not only more accurate, but more widely accessible.

Piezoelectric materials such as piezoceramics, polymers (PVDF, *etc.*), quartz, and ZnO, have been widely used for sensing and actuating.^{6–8} As a category of piezoceramics, the lead zirconate titanate (PZT) series is of particular interest due to its high piezoelectric coefficients and good electro-mechanical coupling. For example, a tactile biosensor has been developed using a resonating PZT element, which measures the

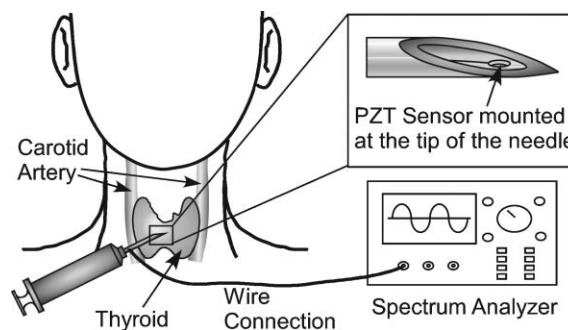


Fig. 1 System diagram of the *in-situ* tissue contrast sensor intended for a thyroid FNA biopsy.

^aEngineering Research Center for Wireless Integrated Microsystems, University of Michigan, 1301 Beal Avenue, Ann Arbor, MI 48109-2122, USA. E-mail: litz@umich.edu; Fax: +1 734-763-9324; Tel: +1 734-647-2040

^bDepartment of Internal Medicine, Division of Metabolism, Endocrinology & Diabetes, University of Michigan, Ann Arbor, MI, USA

firmness of tissue that is in contact with the element by detecting the resonance frequency shift through vibration pick-up.^{9,10} This frequency shift is determined by the acoustic impedance of the tissue, and in this case directly correlated with its firmness. An electrical impedance measurement that benefits from the piezoelectric coupling is also widely used.^{11–13} In another example, when the mechanical boundary condition of a PZT-horn assembly in a geological probe changes by touching different types of rocks, the resonance frequency and the electrical impedance of the assembly change accordingly.¹³

Although extensively used in macro-scale applications, the limitation of conventional micromachining techniques has allowed PZT material to be used for MEMS applications, mostly in the form of films with thicknesses of no more than several microns, which has resulted in degraded material properties and device performance.¹⁴ With the recent development of a customized pair of processes called LEEDUS and SEDUS, bulk PZT materials with superior properties can be patterned lithographically on the micro scale.¹⁵ In these processes, a hard metal tool is fabricated from planar foil by micro electro-discharge machining (μ EDM), and subsequently used to pattern a PZT plate by ultrasonic machining in a batch mode micro ultrasonic machining (μ USM) step.

In this paper, we present a bulk PZT-based, *in-situ* device intended for tissue contrast detection during FNA biopsy of, for example, thyroid nodules.†Intended to complement traditional ultrasound imaging, this device uses a micromachined piezoelectric sensor embedded near the tip of a biopsy needle to distinguish tissue planes. The sensor responds only to tissue in close proximity to the needle tip, in order to provide local information about samples that are collected through the needle tip. The design details are given in Section II. The sensor is fabricated from bulk PZT using a customized process involving SEDUS. The fabrication process is described in Section III, preliminary test results are discussed in Section IV, and are followed by analysis and discussion in Section V.

II. Device design

A PZT disc that is actuated in longitudinal mode for free vibration in the direction of its thickness has both the piezoelectric polarization and the applied electrical field parallel to its thickness. Mechanical resonance for such a disc occurs when its thickness t_0 equals the odd multiples of half of the vibration wavelength, $\lambda/2$, or equivalently when:

$$f_{(n)} = \frac{n \cdot v_0}{2t_0}, \quad n = 1, 3, 5 \dots \quad (1)$$

where $f_{(n)}$ is the n th resonance frequency, $v_0 = \lambda \cdot f_{(n)}$ is the vibration velocity in the material, and n is a positive integer that represents the harmonic number. Due to the piezoelectric effect of the disc, these mechanical resonances correspond to a series of electrical impedance peaks of the PZT disc, and the mechanical resonance frequency, $f_{(n)}$, is equal to the

anti-resonance frequency, $f_{a(n)}$, of the electrical impedance for the disc in this thickness longitudinal driving mode (also referred to as the maximum impedance frequency f_m).^{18,19} The thickness of the PZT disc t_0 will thus determine the location of the impedance peaks on the spectra, and the diameter of the disc, R , should be several times larger than t_0 , in order to reduce the cross-coupling from the lateral wave resonance mode by reducing the lateral resonance frequency. When the mechanical boundary conditions, such as mass and elastic loading, are changed by contact with the materials to be tested, the mechanical resonance of the PZT disc will change accordingly. This is transduced into changes in the electrical impedance peaks of the PZT disc, and can be monitored by measuring the electrical impedance spectra.

The lumped-element Butterworth–Van Dyke (BVD) equivalent circuit can be used to model the electrical characteristics of the PZT disc in the absence of loading.^{18,20,21} A modification to this original BVD circuit is necessary to accommodate the loading effect as shown in Fig. 2(a). Specifically, inductors $L_{m(n)}$ are used to model the mass loading, such as a diaphragm attached to a piezoelectric sensor. The clamped capacitance between the two electrodes of the disc is denoted C_0 , and an infinite number of series RLC_n ($n = 1, 3, 5 \dots$) motional branches are connected in parallel. The first branch of R , L , and C_1 corresponds to the fundamental resonance mode, and the n th branch of R , L , and C_n represents the n th mode defined by eqn (1). The n th anti-resonance frequency $f_{a(n)}$ and resonance frequency $f_{r(n)}$ of the measured electrical impedance for the original BVD circuit without loading inductance $L_{m(n)}$ are:

$$f_{a(n)} = f_{(n)} = \frac{1}{2\pi\sqrt{LC_n}}, \quad n = 1, 3, 5 \dots \quad (2)$$

$$f_{r(n)} = \frac{1}{2\pi\sqrt{LC_n \frac{C_0}{C_0 - C_n}}}, \quad n = 1, 3, 5 \dots \quad (3)$$

The circuit elements are related to the physical parameters of the PZT disc by:

$$C_0 = \frac{\epsilon \cdot A}{t_0} \quad (4)$$

$$C_n = \frac{8k_t^2}{n^2\pi^2} C_0, \quad n = 1, 3, 5 \dots \quad (5)$$

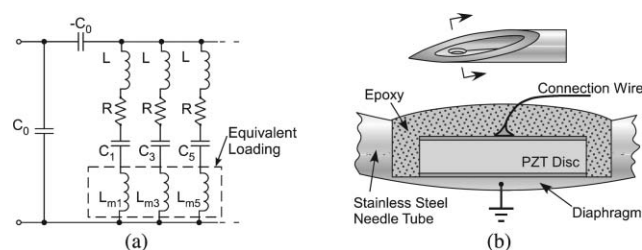


Fig. 2 (a) The lumped-element BVD equivalent circuit for a piezoelectric resonator in longitudinal vibration mode modified to account for tissue loading. The original BVD circuit for such a piezoelectric resonator in free resonance can be restored by removing the $L_{m(n)}$ equivalent loading inductors. (b) Schematic diagram of the tissue contrast sensor.

† Portions of this paper have appeared in conference abstract form.^{16,17}

$$L = \frac{1}{4\pi^2 f_{a1}^2 C_1} \quad (6)$$

$$R = \frac{\eta_0}{\rho_0 v_0^2 C_1} \left(\frac{f}{f_{a1}} \right), \quad n = 1, 3, 5 \dots \quad (7)$$

where ε is the permittivity of the piezoelectric layer; A and t_0 are the area and thickness of the PZT disc, respectively; k_t^2 is the electromechanical coupling constant determined by material properties including piezoelectric constant, stiffness, and permittivity of the piezoelectric material; v_0 and η_0 are the acoustic velocity and viscosity of the piezoelectric layer, respectively; and ρ_0 is the density of the piezoelectric layer. As shown in eqns (2) and (3), both $f_{a(n)}$ and $f_{r(n)}$ are related to motional parameters L and C_n , which are coupled with mechanical boundary conditions, so either one can be used to monitor the resonance change. However, the anti-resonance modes, $f_{a(n)}$, are preferred for this longitudinal piezoelectric coupling because it is fundamentally related only to the thickness of the disc, and less affected by circuit parameters such as variation of C_0 due to parasitic capacitances.²²

The inductors $L_{m(n)}$ that represent loading,^{23,24} are related to the physical parameters of the PZT disc and the added mass by

$$L_{m(n)} = \frac{4f_{a1}^2 L \rho_m t_m}{n \rho_0 v_0}, \quad n = 1, 3, 5 \dots \quad (8)$$

where ρ_m and t_m are the density and thickness of the added mass layer, respectively. The thickness, t_m , should be as small as possible, since it is inversely proportional to the sensitivity of the sensor to any additional mass loading on the diaphragm.²³ This modified BVD circuit model is also used in Section V to describe the equivalent loading provided by tissue.

A preliminary scheme for the *in-situ* detection of tissue contrast during biopsy is illustrated in Fig. 1. A PZT sensor is integrated at the tip of the needle and is connected to a spectrum analyzer for real-time impedance measurement, thus providing information of the tissue contrast during biopsy. Fig. 2(b) shows a schematic of the proposed device. The PZT disc is located within a cavity micromachined into the wall of the needle near the tip, and against a diaphragm which is retained at the bottom of the cavity. The thickness of the diaphragm is non-uniform because of the cylindrical shape of the needle. The metal needle serves as a ground plane for one electrode of the PZT sensor. The second lead, which is to the top of the PZT disc, is a flexible, insulated copper wire that extends along the inside of the needle. Epoxy is used to provide electrical insulation and to seal the device.

The sensor is designed to respond to tissue that is in contact with the diaphragm and in close proximity to the probe as it is inserted during a biopsy procedure. Different tissue types have different densities and elastic properties. The mass loading and elastic loading to the diaphragm, and thereby the vibrational characteristics of the diaphragm, change accordingly. This changes the mechanical boundary conditions of the PZT disc, which is transduced into a change of electrical impedance by the piezoelectric effect, and subsequently detected by the

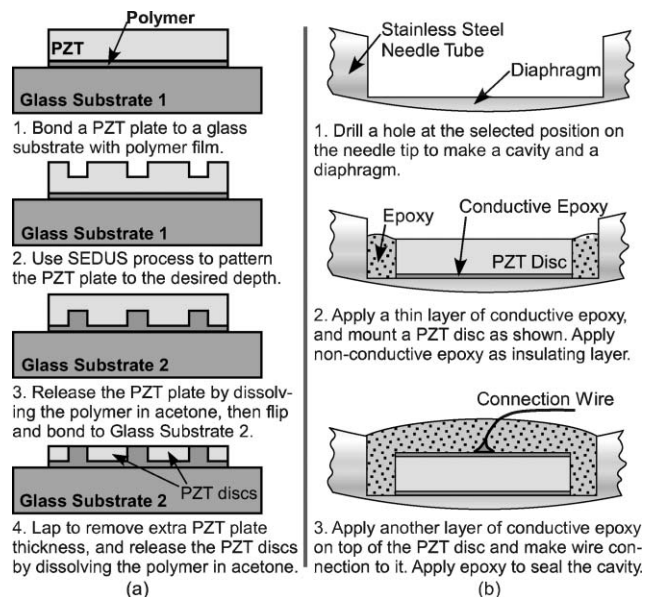


Fig. 3 Diagram of the fabrication process flows for: (a) PZT discs; (b) the *in-situ* tissue contrast sensor at the tip of a biopsy needle.

impedance spectrum analyzer, thus providing a measure of tissue contrast.

III. Device fabrication

The fabrication process for the PZT disc is shown in Fig. 3(a). A bulk PZT-5H plate (Piezo Systems, Inc., USA), which has attractive material properties for sensor applications, is bonded to a glass substrate by a polymer. The SEDUS process,¹⁵ so called because it combines serial mode μ EDM and batch mode μ USM, is performed to fabricate disc-shaped structures on the PZT plate. In this, serial mode μ EDM is used to define simple patterns on a steel microtool by the “writing” movement of a wire electrode. The microtool is then used in batch mode μ USM to transfer the patterns onto ceramic substrates with the help of abrasive slurry. For complex patterns, the steel microtool can be prepared by batch mode μ EDM. Instead of the tip of a wire, the electrode is a pattern of electroplated copper formed on the surface of a microchip. This is used as a “cookie cutter” against a planar steel structure, which subsequently serves as the tool for the ultrasonic machining of ceramics. This process sequence is called LEEDUS, which stands for lithography, electroplating, batch mode μ EDM and μ USM. While it is more complicated than SEDUS, it offers higher throughput and feature uniformity. After machining, the PZT plate is then released by dissolving the polymer, flipped over and bonded again to a second glass substrate. The discs are released by lapping away the extra thickness of the plate and dissolving the bonding polymer. Fig. 4(a) shows a released PZT disc with a diameter of 200 μ m and a thickness of 50 μ m.

The interior apex of the biopsy needle is machined by μ EDM to form the cavity and the diaphragm (Fig. 4(b)), and the PZT element is inserted as illustrated in Fig. 3(b). The cavity diameter and depth are 300 μ m and 150 μ m, respectively. This results in a diaphragm, with a thickness

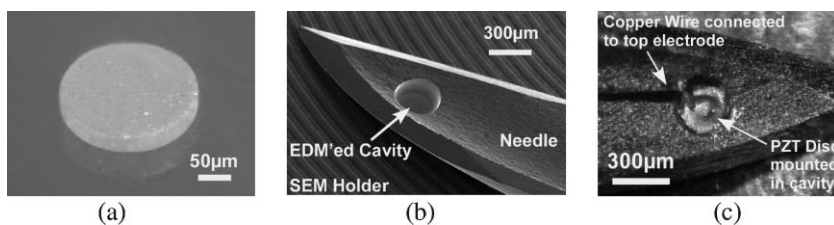


Fig. 4 (a) Photograph of a released PZT disc, batch fabricated by the SEDUS process using batch μ USM to transfer a pattern which was defined by serial μ EDM. Diameter: 200 μ m; thickness: 50 μ m. (b) SEM photograph of μ EDM'd biopsy needle tip with a cavity for mounting a PZT sensor. Cavity diameter: 300 μ m; depth: 150 μ m; corresponding diaphragm thickness: 10–36 μ m. (c) Photograph of a finished device, before sealing epoxy is applied. A coated copper wire is used to make the connection to the top electrode of the PZT disc. The stainless steel needle body is used as a ground.

varying from 10 to 36 μ m, on the 20-gauge needle. A thin layer of conductive epoxy is used to attach the PZT disc to the bottom of the cavity, as well as to attach the lead wire to the top surface of the disc. Non-conductive epoxy is then applied as an insulating layer and sealing material. Fig. 4(c) shows a photograph of the final device with a lead connection to the top electrode, immediately before applying the sealing epoxy.

IV. Experimental

The fabricated devices were tested by penetrating the biopsy needle into: (A) a training arrangement for a thyroid FNA biopsy; (B) porcine tissue consisting of fat and muscle layers; and (C) oil samples and saline solutions of various concentrations, which provided a method for calibrating the device. An HP4195 spectrum analyzer was used to obtain impedance spectra and monitor the change in its resonance peaks.

A. Biopsy training set-up

Fig. 5(a) illustrates a procedure that is sometimes used for training healthcare professionals in thyroid FNA biopsy: a pickled olive simulates the thyroid nodule, while an Aquaflex[®] ultrasound gel pad (Model 04-02 from Parker Labs, Inc., USA) and a dampened sponge simulate the surrounding tissue. Fig. 5(b) shows a typical sensor response as the biopsy needle advances into the sample. A resonance mode with a relatively high frequency and large quality factor (Q) was selected for testing. When the needle was inserted from free space into the ultrasound gel pad, the resonance frequency dropped from 176 MHz to 154 MHz. Both the resonance frequency and the

peak impedance decrease gradually with the advancement of the needle into the gel pad. After the needle tip reaches the olive, the resonance frequency stays almost constant while the impedance peak magnitude increases with advancement into the olive. From the gel pad surface to the olive, the total frequency decrease is ≈ 4 MHz from the initial 154 MHz, and the magnitude decreases by $\approx 800 \Omega$ from the initial 2 k Ω . This kind of shift does not occur if the olive is missing, and these electrical characteristics are thereby indicative of a tissue contrast between the olive and the gel pad, which emulate a thyroid nodule and the surrounding tissues, respectively.

B. Porcine tissue

The following test involved samples of porcine fat and muscle tissue. The needle was first inserted, from free space, directly into either fat or muscle tissue to separately study the sensor response to each kind of tissue. The results are shown in Fig. 6(a). While the resonance frequency drops as the needle is inserted into either tissue, the slope is smaller in muscle tissue. The impedance peak magnitude drops with increasing insertion depth in the fat, but increases in the muscle. These frequency and magnitude changes are possibly due to signal attenuation or stray capacitance caused by the surrounding tissue, and constrain the sampling depth at which the sensor can be effective. However, as can be seen in Fig. 6(a), this device shows clear contrast between fat and muscle up to a depth of >15 mm, which is adequate for thyroid and other superficial biopsies.

The device was also tested with layered samples of porcine fat and muscle tissue, and the results are shown in Fig. 6(b).

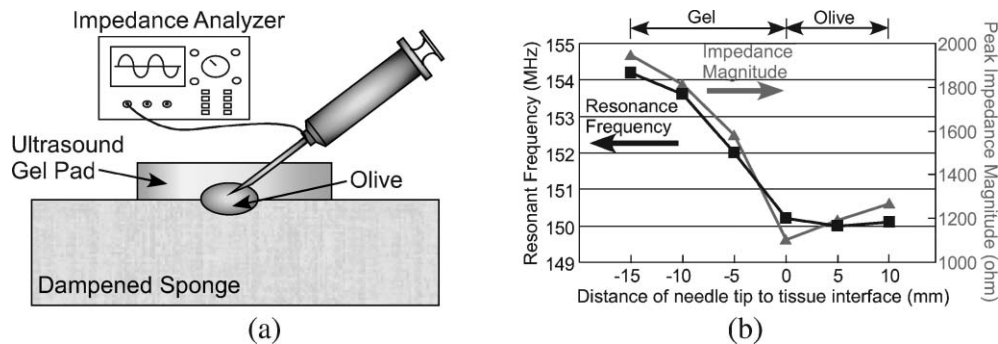


Fig. 5 (a) Schematic diagram showing the biopsy training set-up for thyroid biopsy that was used in the first set of tests. (b) Measured resonance frequency and peak magnitude of the PZT electrical impedance vs. proximity to tissue interface. Once the tip moved into the olive, the resonance frequency remained almost constant while the peak magnitude started increasing.

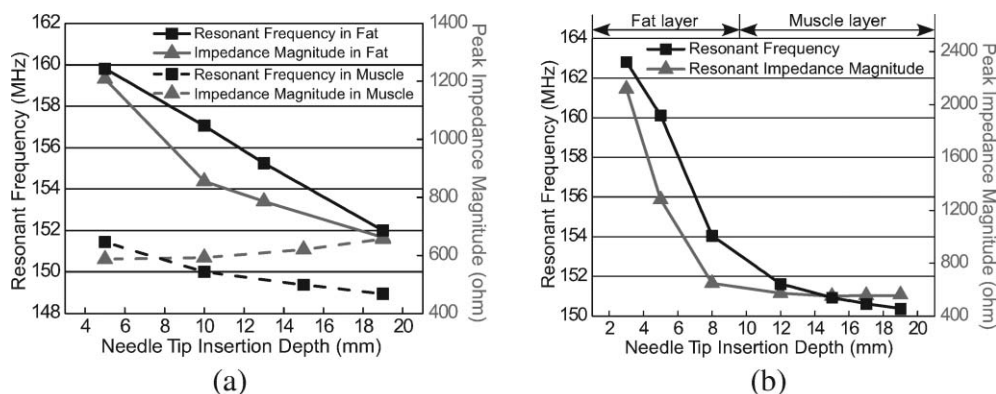


Fig. 6 Measured resonance frequency and peak magnitude of the PZT electrical impedance vs. needle tip insertion depth: (a) from free space directly into porcine fat or muscle tissue; (b) from porcine fat layer to muscle layer.

Table 1 Test results and acoustic properties of samples^a

Samples	Δf /MHz	Density/kg m ⁻³	Sound velocity/m s ⁻¹	Acoustic impedance $Z_a/10^6$ kg m ⁻² s ⁻¹	Equivalent loading inductance $L_{eq5}/10^{-7}$ H
a. Saline-1% ²⁶	22.2	1005	1507	1.515	8.98
Saline-2% ²⁶	22.8	1012	1518	1.537	9.24
Saline-3.5% ²⁶	23.3	1023	1534	1.570	9.44
b. Porcine muscle ²⁷	23.6	1040	1568	1.630	9.57
c. Porcine fat ²⁷	15.2	970	1470	1.426	6.14
d. Body oil ²⁸	1.9	821	1430	1.174	1.68
e. Mineral oil ²⁸	2.0	825	1440	1.188	1.71
f. Peanut oil ²⁸	2.9	914	1436	1.313	1.98

^a Citations indicate sources for density and sound velocity data.

Both the resonance frequency and the impedance peak magnitude decrease gradually as the needle is inserted into the fat tissue. Then, at the insertion depth of about 9 mm, where the needle passes into a muscle layer, the impedance peak magnitude stops dropping, while the resonance frequency further drops with a much smaller slope ($\approx 1/5$ of that in fat). From the fat surface to the muscle, the total frequency change is ≈ 13 MHz from the initial 163 MHz, and magnitude changes about 1600 Ω from the initial 2100 Ω . When the results in Fig. 6 (a) and (b) are compared, similar impedance characteristics can be observed for each kind of tissue. This confirms that the characteristics shown in Fig. 6 demonstrate the tissue contrast between porcine fat and muscle.

C. Saline solution and oils

For the purpose of device calibration and modeling, the sensor was tested with samples that have known and controlled acoustic impedance (Z_a). These are oil samples and saline solutions of varying concentrations. The sensor response was measured at a needle insertion depth of 5 mm for all cases. The Z_a of these samples ranged over $1.1\text{--}1.6 \times 10^6$ kg m⁻² s⁻¹, with the Z_a of common tissues towards the upper end of this range. In the experiment with saline samples, solution concentrations from 1% to 20% were tested. The measured shift of resonant frequency increased with greater saline concentration when the concentration was smaller than $\approx 3.5\%$, and remained approximately constant when the concentration became greater than $\approx 3.5\%$. This phenomenon is similar to that discussed by Zhang *et al.*,²⁵ and is possibly

due to saturation of available cation binding sites on the sensor diaphragm. The sample properties and experimental results of resonance frequency are summarized in Table 1. These results are used in an empirical tissue contrast model described in Section V.

V. Analysis and discussion

A. The tissue contrast model

The resonance frequency shift (Δf) of the piezoelectric sensor is dependent on both the mass loading effect and elastic properties of the samples. The Z_a of a sample is the product of its density

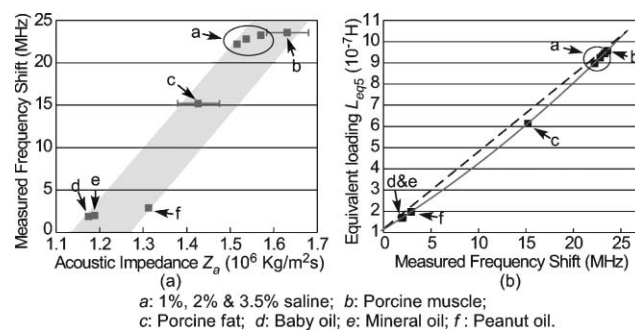


Fig. 7 (a) Measured resonance frequency shift vs. acoustic impedance of the samples. The error bars on the data for porcine samples indicate the lack of certainty in calculated values of acoustic impedance Z_a . (b) Calculated equivalent loading L_{eq5} as a function of frequency shift for the samples. The broken line provides a linear comparison. Data are listed in Table 1.

and acoustic velocity, the latter being further related to the elastic bulk modulus of the material. Thus, an empirical tissue contrast model can be built for the biopsy device by plotting the measured Δf vs. Z_a , as shown in Fig. 7(a). The data used in this plot are from Table 1. The relationship is approximately proportional, as shown in the shaded area, considering the uncertainty in the acoustic properties of the samples.

In Section II, a modified BVD equivalent circuit was described using inductance $L_{m(n)}$ to model the effect of the mass loading of the diaphragm to the PZT disc. To include the tissue loading effect in the model, $L_{m(n)}$ can be extended by adding in series another equivalent loading inductance $L_{eq(n)}$. This additional inductance is an equivalence that includes the effect of both mass and elastic loading. The new anti-resonance frequency for the impedance is therefore:

$$f_{a(n)} = \frac{1}{2\pi\sqrt{(L + L_{m(n)} + L_{eq(n)})C_n}}, \quad n = 1, 3, 5 \dots \quad (9)$$

In the experiments, the 5th harmonic mode (at 176 MHz in air) was found to have a higher Q than the fundamental and 3rd harmonic modes, and was consequently selected for measurement. This is similar to the situation discussed by Zhang *et al.*,²³ and is possibly due to less acoustic energy loss in the 5th harmonic mode than in the 1st and 3rd modes, but the underlying physical reason remains unclear. Therefore, the 3rd RLC_n branch (for the 5th harmonic mode) of the modified BVD circuit is of the most interest. The calculated equivalent loading L_{eq5} for each of the samples, used to build the empirical tissue contrast model, is listed in Table 1 and plotted as a function of the measured frequency shift Δf_{a5} in Fig. 7(b). The two plots in Fig. 7 provide the empirical tissue contrast model (*i.e.*, the relationship of Z_a to Δf_{a5}) and the relationship of L_{eq5} to Δf_{a5} . These relationships can be used with the modified BVD circuit model to relate the physical parameters of the device and samples to Δf for design and optimization of the sensor.

B. Transmission line assessment

The transmission line characteristics of the stainless steel needle tube, along with the inner copper wire, are not related to tissue properties and are thus not required to detect a contrast in the tissue. However, they are worth considering because they can affect the measured electrical impedance. In the absence of a liquid within the biopsy needle, *i.e.* while the needle is approaching the target, the connection wire to the sensor and the surrounding needle structure can be approximately modelled as a coaxial line. An equivalent circuit model

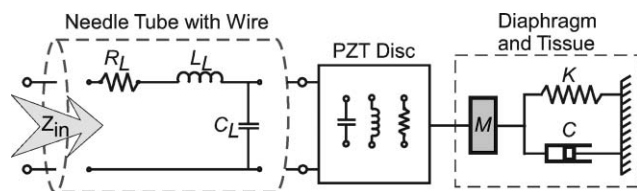


Fig. 8 The circuit model for the transmission line analysis carried out to evaluate the effect of the needle tube and the copper wire on the measured impedance characteristics. A coaxial line model was used and the PZT disc was replaced by an equivalent static capacitor.

is shown in Fig. 8. In this model, the PZT disc can be replaced with an equivalent static capacitor for the transmission line analysis, so the piezoelectric effect is not considered. The extension wire that connects the needle tube to the impedance analyzer is neglected because it can be compensated for during the measurement. According to the classic transmission line theory for a terminated lossy coaxial line,²⁹ the input impedance Z_{in} is:

$$Z_{in} = Z_0 \frac{Z_p + Z_0 \tanh \gamma l}{Z_0 + Z_p \tanh \gamma l} \quad (10)$$

where Z_p is the impedance of the equivalent static capacitor replacing the PZT disc, and the capacitance value is 20 pF for this analysis; l is the length of the coaxial line and is equal to 25 mm; Z_0 and γ are the transmission line characteristic impedance and the complex propagation constant, respectively, and are both related to the transmission line parameters R_L , C_L , and L_L by equations found in the classic transmission line theory. These parameters R_L , C_L , and L_L are further related to the physical parameters of the coaxial line, including the radius of the copper wire r_a which is 25 μm , and the inner radius of the needle tube r_b which is 292 μm . Since air is used as the dielectric material for this coaxial line model, its permittivity and permeability properties are used in the analysis.

According to this approximate analysis, the calculated input impedance Z_{in} of this model drops smoothly within the frequency range of interest, and the length of the equivalent coaxial cable can be considered much shorter than the calculated transmission line characteristic wavelength. Thus, the effect of the needle tube can be basically ignored for our purpose. The calculated ratio of the power delivered to the PZT disc through the needle tube and copper wire varies almost linearly with frequency from $\approx 95\%$ at 1 MHz to $\approx 65\%$ at 160 MHz.

C. Penetration depth

The working depth of the device is limited by the length of the needle to 25 mm, and as discussed in the porcine tissue tests in Section IV, is also limited by the degradation of sensor performance due to possible signal attenuation or stray capacitance. The working depth of the current device is enough for the anticipated use in shallow FNA procedures such as thyroid biopsy, the working depth of which is usually <15 mm. In order to be used in deep tissue biopsies, such as those for breast or celiac organs, longer needles are required. This increased needle length and thus greater insertion depth into tissues can cause further degradation of sensor performance, and will be investigated in future efforts.

D. Scaling consideration

In this effort, a $\text{\O}200$ μm PZT disc was embedded in a $\text{\O}300$ μm cavity in a 20-gauge biopsy needle. For needles of smaller gauge, which are sometimes needed in biopsy procedures, the wall thickness of the needle tube reduces, while the curvature of the wall increases, requiring the size of the PZT disc to be scaled down accordingly. For example, a 27-gauge needle has an outer diameter of only 406 μm and wall thickness of 102 μm . The LEEDUS/SEDUS process that has been used to fabricate

the discs has the capability of handling feature sizes as small as 25 μm ,¹⁵ and can provide PZT elements with diameters much smaller than the current 200 μm value. However, the integration of these discs onto the biopsy needle can be a problem when the size is too small to handle manually or by a pick-and-place machine. A new approach for this integration is needed in this case.

VI. Conclusions

A micromachined bulk PZT sensor has been integrated into a cavity at the tip of a biopsy needle to aid in real time tissue differentiation during FNA biopsy, providing information that is complementary to any imaging method which may be used concurrently to guide the procedure. The batch fabricated PZT disc has a 200 μm diameter and is located on a diaphragm formed with the cavity. Devices were tested in a simulated scheme for physician training, as well as in porcine tissue consisting of fat and muscle layers. In both types of tests, the frequency and magnitude of an impedance resonance peak showed tissue-specific characteristics as the needle was inserted into the tissue. For example, in the porcine tissue sample, the frequency shifted ≈ 13 MHz as the needle moved from fat to muscle tissue. Additional measurements with saline solutions and oil samples were carried out to build an empirical tissue contrast model, which showed a proportional relationship between the frequency shift and sample acoustic impedance. These results and subsequent analyses indicate that the proposed device is promising in providing effective guidance to the physician during an FNA biopsy. Issues that need further investigation, such as penetration depth limitation and the effect of local tissue trauma to the PZT response during needle insertion, will be addressed in future efforts. Using schemes similar to the one described, it is also possible to integrate various types of other sensors on biopsy and surgical tools, providing additional information that can be of interest to physicians, e.g., complementary tumor location during excision surgery.

Acknowledgements

This work was supported primarily by the Engineering Research Centers Program of the National Science Foundation under Award Number EEC-9986866. Facilities used for this research include the Michigan Nanofabrication Facility (MNF) operated by the Solid-State Electronics Laboratory (SSEL) at the University of Michigan.

References

- 1 J. T. Johnson and L. Zimmer, *Fine-needle aspiration of neck masses*, eMedicine World Medical Library from WebMD, 2005, <http://www.emedicine.com/ent/topic561.htm>.
- 2 Fine-needle aspiration biopsy, in *Currents: Physician-To-Physician Clinical Resource*, ed. Z. Anguelov, 2002, 3(2), <http://www.ui-healthcare.com/news/currents/index.html>.
- 3 F. Pacini and L. J. De Groot, Thyroid neoplasia, in *The Thyroid and its Diseases*, W. B. Saunders Company, 6th edn, 1996, updated online at <http://www.thyroidmanager.org>, May 2004.
- 4 S. Takashima, H. Fukuda and T. Kobayashi, Thyroid nodules: clinical effect of ultrasound-guided fine-needle aspiration biopsy, *J. Clin. Ultrasound*, 1994, 22(9), 535–542.
- 5 H. Gharib and J. R. Goellner, Fine-needle aspiration biopsy of the thyroid: an appraisal, *Ann. Intern. Med.*, 1993, 118(4), 282–9.
- 6 G. Gautschi, *Piezoelectric Sensorics: Force, Strain, Pressure, Acceleration and Acoustic Emission Sensors, Materials and Amplifiers*, Springer, New York, 2002.
- 7 K. Uchino, *Piezoelectric actuators and ultrasonic motors*, Kluwer Academic, Boston, 1997.
- 8 Q. -X. Su, P. Kirby, E. Komuro, M. Imura, Q. Zhang and R. Whatmore, Thin-film bulk acoustic resonators and filters using ZnO and lead-zirconium-titanate thin films, *IEEE Trans. Microwave Theory Tech.*, 2001, 49(4, pt. 2), 769–78.
- 9 S. Omata and Y. Terunuma, New tactile sensor like the human hand and its applications, *Sens. Actuators, A*, 1992, 35(1), 9–15.
- 10 Axiom Co. Ltd. Website, <http://www.axiom-j.co.jp>.
- 11 J. W. Ayres, F. Lalande, Z. Chaudhry and C. A. Rogers, Qualitative impedance-based health monitoring of civil infrastructures, *Smart Mater. Struct.*, 1998, 7, 599–605.
- 12 K. K. Tseng and L. Wang, Impedance-based method for non-destructive damage identification, *J. Eng. Mech.*, 2005, 131(1), 58–64.
- 13 Z. Chang, S. Sherrit, X. Bao and Y. Bar-Cohen, In-situ rock probing using the ultrasonic/sonic driller/corer, in *Proc. SPIE Smart Structures Conference*, vol. 5056, San Diego, 2003, pp. 567–573.
- 14 D. L. Polla and L. F. Francis, Ferroelectric thin films in microelectromechanical systems applications, *MRS Bull.*, 1996, 59.
- 15 T. Li and Y. B. Gianchandani, A micromachining process for die-scale pattern transfer in ceramics and its application to bulk piezoelectric actuators, *IEEE/ASME J. Microelectromech. Syst.*, 2006, 15(3), 605–612.
- 16 T. Li, R. Y. Gianchandani and Y. B. Gianchandani, A bulk PZT microsensor for in-situ tissue contrast detection during fine needle aspiration biopsy of thyroid nodules, in *Proceedings of the IEEE International Conference on Micro Electro Mechanical Systems (MEMS 2006)*, Istanbul, 2006, pp. 12–15.
- 17 T. Li and Y. B. Gianchandani, An empirical model for a piezoelectric tissue contrast sensor embedded in a biopsy tool, in *Proceedings of the 10th International Conference on Miniaturized Systems for Chemistry and Life Sciences (μ TAS2006)*, Tokyo, 2006, pp. 837–839.
- 18 T. Ikeda, *Fundamentals of Piezoelectricity*, Oxford University Press, New York, 1990.
- 19 *IEEE Standard on Piezoelectricity*, ANSI/IEEE Std. 176-1987, withdrawn in 2000.
- 20 *Guide to Dynamic Measurements of Piezoelectric Ceramics with High Electromechanical Coupling*, IEC Standard Publication 483, 1976.
- 21 W. Pan, P. Soussan, B. Nauwelaers and H. A. C. Tilmans, A surface micromachined electrostatically tunable film bulk acoustic resonator, *Sens. Actuators, A*, 2006, 126(2), 436–46.
- 22 R. E. McKeighen, Design guidelines for medical ultrasonic arrays, *Proc. SPIE—Int. Soc. Opt. Eng.*, 1998, 3341, 2–18.
- 23 H. Zhang and E. S. Kim, Micromachined acoustic resonant mass sensor, *IEEE/ASME J. Microelectromech. Syst.*, 2005, 14(4), 699–706.
- 24 S. J. Martin, V. E. Granstaff and G. C. Frye, Characterization of a quartz crystal microbalance with simultaneous mass and liquid loading, *Anal. Chem.*, 1991, 63, 2272–81.
- 25 H. Zhang, M. S. Marma, E. S. Kim, C. E. McKenna and M. E. Thompson, Implantable resonant mass sensor for liquid biochemical sensing, in *Proceedings of the IEEE International Conference on Micro Electro Mechanical Systems (MEMS 2004)*, 2004, pp. 347–50.
- 26 F. T. Gucker, C. L. Chernick and P. Roy-Chowdhury, A frequency-modulated ultrasonic interferometer: adiabatic compressibility of aqueous solutions of NaCl and KCl at 25 °C, *Chemistry*, 1966, 55, 12–19.
- 27 D. J. Dowsett, P. A. Kenny and R. E. Johnston, *The Physics of Diagnostic Imaging*, Chapman and Hall Medical, New York, 1998.
- 28 A. R. Selfridge, Approximate material properties in isotropic materials, *IEEE Trans. Sonics Ultrason.*, 1985, SU-32(3), 381–94.
- 29 D. M. Pozar, *Microwave Engineering*, John Wiley & Sons, Inc., Hoboken, NJ, 3rd edn, 2005.